J. Inst. Eng. India Ser. D (May–August 2024) 105(2):675–688
https://doi.org/10.1007/s40033-023-00527-1

ORIGINAL CONTRIBUTION

Analysing Microstructure and Hardness of SS-304 Under Annealed, Normalized, Quenched and Step Cooled Conditions

Saurabh Dewangan[1] · **Shrey Mishra**[1]

Received: 10 June 2023 / Accepted: 14 July 2023 / Published online: 24 July 2023

Abstract SS-304 is austenitic stainless steel that possesses γ-austenite, δ-ferrite, and different carbides at room temperature. The properties of austenitic steel can be varied by cold forming because it is hardly responsive to thermal treatment. To critically analyze the microstructural attributes of SS-304, the present work deals with seven different heat treatment techniques. The properties of heat-treated samples were analyzed based on the properties of the untreated or 'original' sample. The samples were heated at 900 °C for 1 h and then cooled at seven different media, namely, Water, Oil, Air, Sand, Brine, Air + water, and Air + oil. The microstructural analysis was carried out by using light optical microscopy (LOM), field emission scanning electron microscopy (FESEM-back scattered detectors), elemental mapping, energy dispersive spectroscopy (EDS), and X-ray diffraction (XRD). Also, the micro-hardness of all the samples was tested. The purpose of this work is to check the effect of heat treatment on the microstructural appearance of the SS-304. Based on that, the hardness and corrosive degradation of the steel samples were also analyzed. LOM images showed a negligible difference among the samples while the FESEM images were capable to show the formation of M23C6 at the γ-δ interface. In addition, another phase-σ was recognized in the view of previous literature. A little amount of pitting was noticed in the γ-phase of Brine and Water quenched samples. The elemental mapping showed a slight variation in Wt% of Cr in some of the heat-treated samples. As a result of water quenching and Air + water stepped cooling, the hardness of the samples got increased by 7.4% and 5.6% respectively.

Keywords SS-304 · Heat treatment · Quenching · Annealing · Normalizing · Stepped cooling · γ and δ matrix · Pitting

Introduction

Stainless steel (SS) or corrosion-resistant steel imparts a minimum amount of 11% chromium. This type of steel can be divided into four categories: ferritic, martensitic, austenitic, and austenitic + ferritic (or duplex) SS. These steels can be distinguished according to their microstructural appearance at room temperature [1]. Further, the microstructure orientation is influenced by alloy composition. Although SS is known for its corrosion-resistant properties, other properties like fracture toughness and oxidative resistance can be altered by the addition of other alloying elements. For example, Nb and Ti improve the IGC (inter-granular corrosion) resistance property of SS by absorbing the carbon to form carbides. Machinability is enhanced by sulphur which is responsible to form manganese sulphide. Nitrogen helps to improve the strength of the steel. Because of its good surface finish and anti-corrosion properties, SS is used in various industries like chemical, aerospace, medical, pharmaceutical, food processing, and even household as well as jewelry works [2].

Metallography of stainless steel becomes important for quality control throughout the production process. The research area includes grain size measurement, identification, and evaluation of the distribution of γ, δ, α′, σ, and various carbides (like $M_{23}C_6$), etc. The corrosion and oxidation measurement has also been an interesting topic in the

✉ Saurabh Dewangan
saurabh22490@gmail.com

Shrey Mishra
shrey.199402059@muj.manipal.edu

[1] Department of Mechanical Engineering, Manipal University Jaipur, Jaipur, Rajasthan 303007, India

past decade. The austenitic grade contains 17–24% of Cr, 9–25% Ni, 2–4% Mo and a little proportion of Ti and Nb which forms carbide in the matrix [3]. SS possesses good malleability, formability, and machinability. The property of SS is influenced by cold working and usually, it is not affected by heat treatment. Instead, the quenching may lead to the formation of a soft structure. The high-temperature exposure of nearly 700 °C leads to the formation of carbides in the γ-matrix. Further, this condition is responsible for the reduction of Cr in γ-matrix and thereby enhancement of IGC [4, 5]. Light optical microscope (LOM), scanning electron microscope (SEM), and transmission electron microscopy (TEM) are used to analyze the structure and phases of stainless steel [6].

In general, it has been noticed that austenitic SS is not influenced by heat treatment, rather a softness is seen due to quenching [2]. Therefore, in the present work, various heat treatment techniques have been applied to the SS-304 samples to investigate the possible changes in microstructure and hardness. For this purpose, the steel samples were heated at 900 °C. LOM, SEM, and XRD have been used under study. Also, for hardness, a micro-Vickers hardness test has been carried out. The Fe–Cr phase diagram for austenitic stainless steel indicates that recrystallization of metal and stress relief occurs at a temperature of 900 °C. At this temperature, there is no phase transition. This indicates that the microstructure of SS-304 at room temperature, i.e., γ + δ, will not change at 900 °C. For complete phase conversion, annealing temperatures > 1000 °C are utilized for industrial applications. The phases were left unaltered during the heat treatment and subsequent analysis in this work.

Literature Review

In a recent study, the mechanical behavior and microstructural features of welded joints of SS-304 were evaluated. In comparison to the quenched plate, the welded part of the tempered plate showed a 150% and 3% increase in toughness and yield strength respectively with a decrement in hardness and ultimate tensile strength. Furthermore, tempering reformed the grain structure, generating twins in the base metal and lathy δ ferrite & γ + δ lamella in the heat-affected zone. The martensite that formed in the quenched specimen was transformed into a fine γ + δ matrix [7]. AISI 304 steel was investigated microscopically when it was near-rapidly directionally solidified. As a result, δ ferrite dendrites were observed with well-developed side branches and inter-dendritic austenite under a temperature gradient. At a higher growth rate, the microstructure transformed into a coupled growth structure of thin lamellar ferrite and austenite. In this study, growth rate and temperature gradient were found to be critical factors in determining the microstructure [8]. The fabrication of ultrafine microstructures was carried out in SS304 polycrystalline materials through a high-pressure self-heating melting and quenching process. By applying pressure quenching, the hardness and yield strength of the samples significantly improved with a reduction in elongation rate. This decrease in elongation was mainly because of the high density of dislocations [1]. A study examines the performance and microstructure of AISI 304 stainless steel that was welded using the MIG process. The results showed that a lower heat input led to a higher ultimate tensile strength in comparison to medium and high heat inputs. An increase in heat input resulted in the coarsening of the grain in the heat-affected zone. Fracture toughness tests revealed a brittle fracture nature, indicating low ductility. The weld zone microstructure was found to have a skeletal δ-ferrite in an austenite matrix with varying ferrite content [9].

The wear resistance of 304 stainless steel was aimed to increase while maintaining its corrosion resistance. To achieve this, a YAG fiber laser was employed to coat the alloy's surface with TiC powder of particle size 3–10 µm. As a result of the cladding process, TiC particles converted into dendritic shapes due to melting and solidification. Further, it was seen that dendrite formation was increasing with traveling speed. It was concluded that a significant improvement in surface hardness and wear resistance was reported during all processing conditions [10]. The.lean duplex- SS (S32101) was analyzed for its microstructural changes at welded joints under post-weld heat-treated conditions. In its as-welded state, the stainless steel had nitride precipitation only in the HAZ. A short isothermal heat treatment of 15 min at 650 °C resulted in numerous nitride precipitates in the parent metal, HAZ, and weld. Extending the holding time to 90 min for all test temperatures encouraged the growth of carbides and nitrides at grain boundaries and inside grains in each zone of the welded joints. However, the presence of inter-metallic σ-phase was not observed in either the parent metal or the welded joints, even after a 90-min heat treatment at 850 °C [11].

In this study, the effect of prolonged annealing on the microstructure and hardness of AISI 310S heat-resistant steel (comprised of 24.3% Cr, 19.3% Ni, 1.8% Mn, 0.21% Mo, and 0.67% Si) was investigated. The steel is commonly used in high-temperature environments. Isothermal annealing was carried out at 800 °C for various durations, ranging from 1 to 1740 h, and microstructural changes and hardness distribution were monitored. SEM and EDS were used to assess the grain structure and fracture mode. The results indicated that the sigma phase precipitated in the γ-matrix and at grain boundaries of it. With an increment in annealing time, the Cr content had increased in the sigma phase. In this stage, Cr was found with a changed morphology of coarse particles which earlier was in the form of fine precipitates. The hardness of the steel increased after 16 h of

annealing and continued to increase with longer annealing times. This was reflected in changes in the fracture surfaces, which were influenced by changes in the content and morphology of the sigma phase [12]. The purpose of this study is to investigate the effects of various heat treatments on the microstructure and thermophysical properties of 1.4462 duplex stainless steel. Four samples were analyzed, including an untreated sample and three heat-treated samples. The first heat treatment consisted of annealing the steel at 1200 °C for one hour, followed by rapid cooling in water. The second treatment was the same as the first but with an additional 4-h annealing at 800 °C and slow cooling in the furnace. The third treatment involved annealing at 900 °C for one hour and slow cooling in the furnace. The resulting ferrite-to-austenite ratios in three samples were 75:25, 65:35, and 44:56, respectively [13]. The X6CrNiMoVNb11-2 super martensitic stainless steel is a unique type of stainless steel that is widely used to produce gas turbine discs. By optimizing the heat treatment process, the mechanical properties of this steel can be tailored to meet specific practical application requirements during advanced composite casting-rolling forming processes. A work aims to investigate the relationship between microstructural attributes and physical properties of this steel after quenching and tempering. The heat treatment process involved the transformation of the martensite phase, where a significant amount of high-density nanophase precipitation was observed. The lamellar martensite had dispersed $M_{23}C_6$ carbides, while the close-packed Ni3Mo and Ni3Nb phases had been created during the tempering process. Oil quenching at 1040 °C and tempering at 650 °C by air-cooling were found ideal conditions for favorable microstructure. This study enhances the understanding of the strengthening mechanism and performance-controlling scheme of martensitic stainless steel during the cast-rolling forming process, leading to better future applications [14]. In a work, the purpose of the investigation was to assess the effect of TiO2 nanoparticles on electroplated mild steel coatings using Ni-Co plating solution. The study focused on examining the material's behavior and corrosion resistance of the composite coatings by introducing varying concentrations of TiO2 sol. into the plating bath. The findings revealed the incorporation of the appropriate concentration of TiO2 sol. into the plating bath resulted in well-dispersed TiO2 nanoparticles in the Ni-Co coating, which led to a significant improvement in the mechanical properties of the coatings. Specifically, the Ni-Co-12.5 mL/L TiO2 coating exhibited the highest level of microhardness, wear resistance and corrosion resistance. Nevertheless, an excessive amount of TiO2sol (more than 12.5 mL/L) added to the electrolyte resulted in the agglomeration of nanoparticles and a porous structure of the coatings, leading to negative effects on their properties [15]. The microstructural analysis of TIG welded stainless steel plates was carried out in a study. It was seen that the second welding pass was responsible for the creation of secondary austenite in the weldment and for making ferrite grains coarse near the fusion line. The other regions shared similar microstructures but had varying amounts of austenite. Microhardness was affected by the distribution of alloying elements. The austenite's hardness exceeded that of the ferrite from the weld metal to the fusion line, but the opposite was true from the fusion line to the base metal. Electrochemical experiments found that the zone with the fusion line was the most susceptible to pitting, followed by the weld metal zone. The surface morphologies corresponded with the electrochemical measurements [16]. The experiment was conducted on 16 mm HSLA steel plates with high heat input (ranging from 3.0 to 6.3 kJ/mm) by adjusting the welding current (ranging from 500 to 700 A) and speed (ranging from 200 to 300 mm/min). The results showed that an increase in heat input led to a coarser grain structure in both the weld metal and heat-affected zone (HAZ). The hardness varied from the center line to the base metal, with the HAZ exhibiting the highest hardness. The hardness of the weld metal was uniform. As the welding current increased and speed decreased (resulting in higher heat input), the hardness decreased, while toughness showed mixed results. An increase in welding current from 500 to 600 A improved toughness, but further increasing it to 700 A reduced toughness. SEM and EPMA were used to examine the fracture modes and the variation of elements in the weld metal and HAZ, respectively [17]. In a study, different processing methods, like, hot-rolling, quenching, and equal-channel angular pressing (ECAP) were applied to low-carbon steel to examine their effects on its microstructure, microhardness, and corrosion resistance properties. The goal was to determine the most suitable processing method. ECAP provided a finer grain structure than quenching methods. Although quenching had improved the anti-corrosion properties of low-carbon steel in an acidic environment, ECAP enhanced the anodic passivation while simultaneously increasing the acid corrosion rate. Based on the results, quenching was determined to be a better option than ECAP for strengthening low-carbon steel in an acidic environment [18]. The microstructural analysis of SS 309 austenitic steel was carried out after applying thermal fatigue cycles at the temperature range of 100◦C- 900 ◦C. Instruments like OM, SEM, and XRD were utilized under study. By increasing the temperature level up to 900 ◦C, a reduction in strength, elongation, and fatigue life was reported. The specimens showed micro-void coalescence because of fatigue failure. The cavity formation was seen at the grain boundaries and twin edges during the fatigue processes. In addition, this high-temperature fatigue process enhanced the oxidation process and thereby oxides were reported on the cracked zones of the specimens. These oxides were further found as the main reasons for the reduction of fatigue life

of the steel [19]. In this study, the Tungsten Inert Gas (TIG) welding process was examined for its efficacy in welding stainless steel grades with similar compositions. The primary objective was to analyze the impact of various welding parameters on the microstructure and mechanical properties of the welds produced. Specifically, the study focused on 310 austenitic stainless steel and evaluated the effect of welding current, filler materials, and welding speed. The results indicated that welds produced with a current of 120A and 309L filler rods had higher tensile strength and fewer defects compared to other welding parameters tested [20].

Materials and Methodology

A total of eight SS-304 samples of dimension 25 × 25 × 2.5 mm were taken. These samples were in cold-rolled condition. Out of them, one sample was kept in its original condition, and seven others were heat treated in an induction furnace. The heating temperature was 900 °C for a period of 1 h. The red-hot samples after one hour of heating are shown in Fig. 1(a). Hot samples were brought out from the furnace one by one. The first sample was buried inside sand for cooling till room temperature. The second sample was kept in atmospheric air. The third and fourth samples were dipped into water and oil for quick cooling. The fifth sample was dipped into brine solution which was prepared by mixing 0.5 kg of salt into 1.5 L of water. The sixth and seventh samples were cooled in two steps- Air + water and Air + oil respectively. The initial 30 s was decided for air cooling and then subsequent cooling of the sixth and seventh samples in water and oil respectively. Overall experimental work has been shown in Fig. 1. For microscopic observation, samples were fixed on two molds so that polishing can be done together. All the samples were highly polished by using sandpapers of various grit sizes and polishing discs. The polished samples were then etched through Kalling (No-2) reagent prior to observation of microstructure on LOM. The microscopic images were captured at two different magnifications- 500X and 1000X. The polished samples were undergone through SEM (backscattered electron detectors) for detecting phases by the dark/bright appearance of different phases. Due to different atomic numbers, various phases appear in different contrast.

The hardness of all the specimens was measured by using a micro-Vickers hardness tester with a load of 300 gm. On each sample, there were four indentations made and an average hardness was calculated.

Microstructural Analysis

(i) By LOM: By using light optical microscopy, images were captured at two different magnifications, i.e., at 500X and 1000X. At 500X, a clear appearance of γ and δ phases could be noted. Also, annealing twins, carbides, and martensite (very less) were also observed. At 1000X, mainly intergranular M23C6 carbide was noted in the images. Some σ-phases were also noted in some cases. σ-phase is usually reported in SS with high Cr content. It has a tetragonal crystal structure that forms at high temperatures. At high temperatures, high Cr stainless steel starts getting unstable. As a result, a new crystalline structure of Fe and Cr, called σ-phase, starts to form. σ-phase is responsible for reducing the corrosion resistance properties of the stainless steel. The microstructural images at 500X and a scale of 100 μm are shown in Fig. 2.

In all the images, the presence of both γ and δ phases could be established by virtue of color contrast. Kalling reagent is a suitable etchant for showing these color contrast. The γ-matrix can be seen a bright appearance while the darker grains are representing δ-ferrite. Figure 2(a) is the image of the original sample which is in cold rolled condition. Both γ and δ are in equiaxed condition. The δ-ferrite is mostly present in stringer form. Various annealing twins could be obtained from the image. A very little amount of martensite (α′) could also be noticed in the γ-matrix. Figure 2(b) is showing the image of a water-quenched sample in which the morphology is similar to the original sample. However, δ-ferrite strings were not as dominant as the original sample. Also, there was no martensite reported in this sample. Figure 2(c) is representing the sample that was quenched in oil. In this, significant twinning was reported in γ grains. The δ-ferrite strings are longer than the original sample. Figure 2 (d) belongs to air cooled sample in which twin formation is not as significant as in oil quenched sample. The rest of the things, δ and γ phases are very similar to previous images. Figure 2(e) is the image of the sand-cooled sample in which twinning is comparatively lesser than that of the original sample. Also, the dark and predominant appearance of the δ-phase is reduced in this case. The δ-stringers are not continuous. Figure 2(f) shows the microstructure of a brine quenched sample in which the δ-phase is larger than the original and quenched samples. There are numerous fine carbides in the γ-matrix. It is because of the conversion of carbon into fine carbides over the γ-matrix. Figure 2(g) is the microstructure of Air (first 30 s) + water (till room temperature) stepped-cooled sample. The microstructural appearance is different from both air and water-quenched samples. Both δ and γ grains are equiaxed in this sample. Intergranular carbide is comparatively larger than that of the brine-quenched sample. δ-ferrite strings almost disappeared in this sample. Figure 2(h) shows the microstructure of Air (first 30 s) + oil (till room temperature) stepped-cooled sample. The δ and γ structure is similar to the oil quenched sample but the γ-matrix in this sample is predominant. δ string is available but it is not continuous.

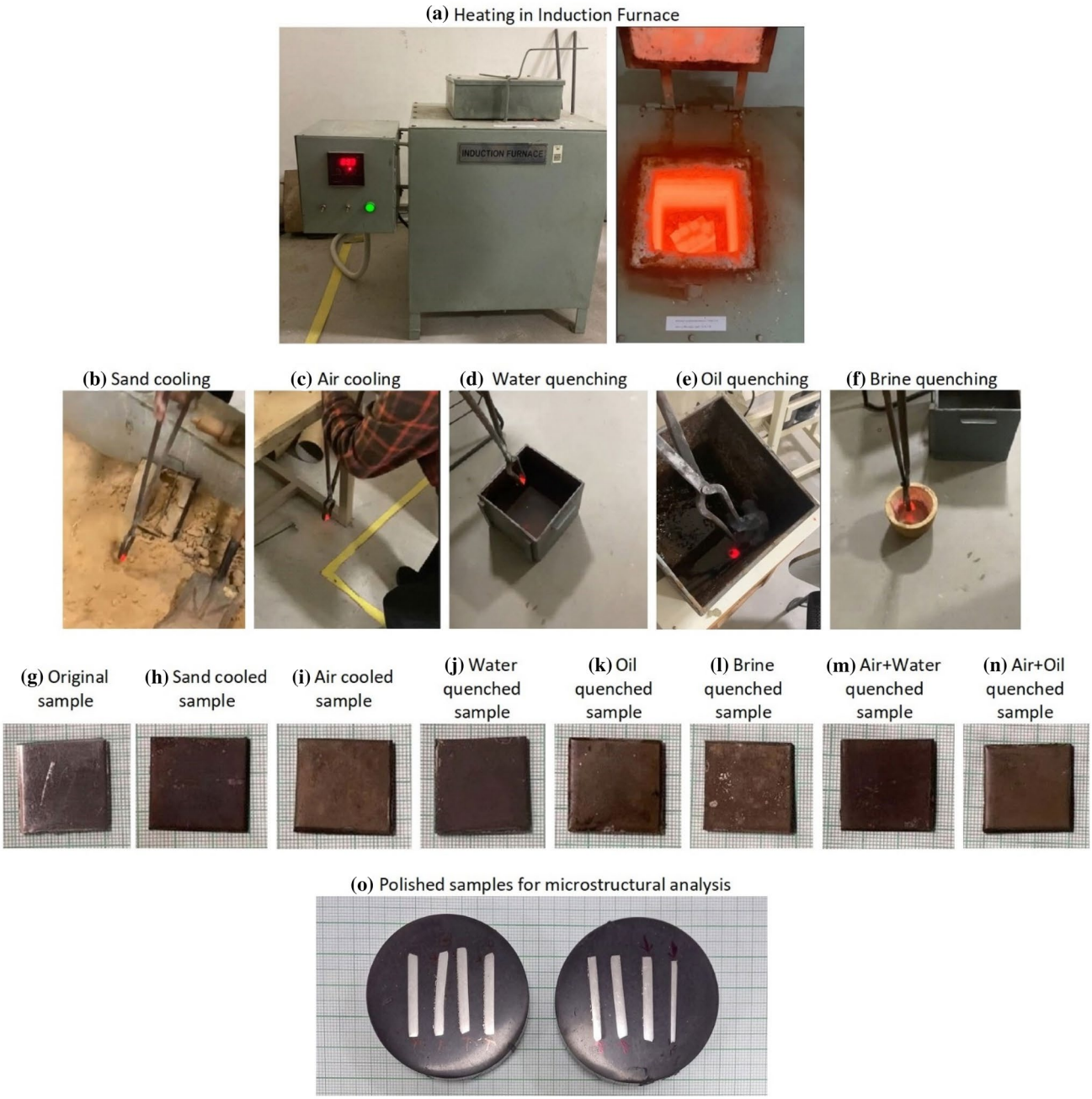

Fig. 1 Experimental detail; **a** Heating seven samples in an Induction furnace; **b–f** Cooling at different media; **g–n** Samples are labeled as per their physical conditions; **o** Polished samples attached on two molds

The commonly observed carbide type in austenitic steel is M23C6, where M can be Cr, Fe, or Mo. During thermal treatment, this carbide may get precipitated at the grain boundary of γ-matrix which further may lead to inter-granular corrosion. To avoid the type of corrosive action, a strong carbide former like Ti can be added to the alloy. The precipitation of M23C6 at the grain boundary may get faster at the temperature range of 650 – 700° C [21]. In the present work, the heat-treating temperature of 900 °C

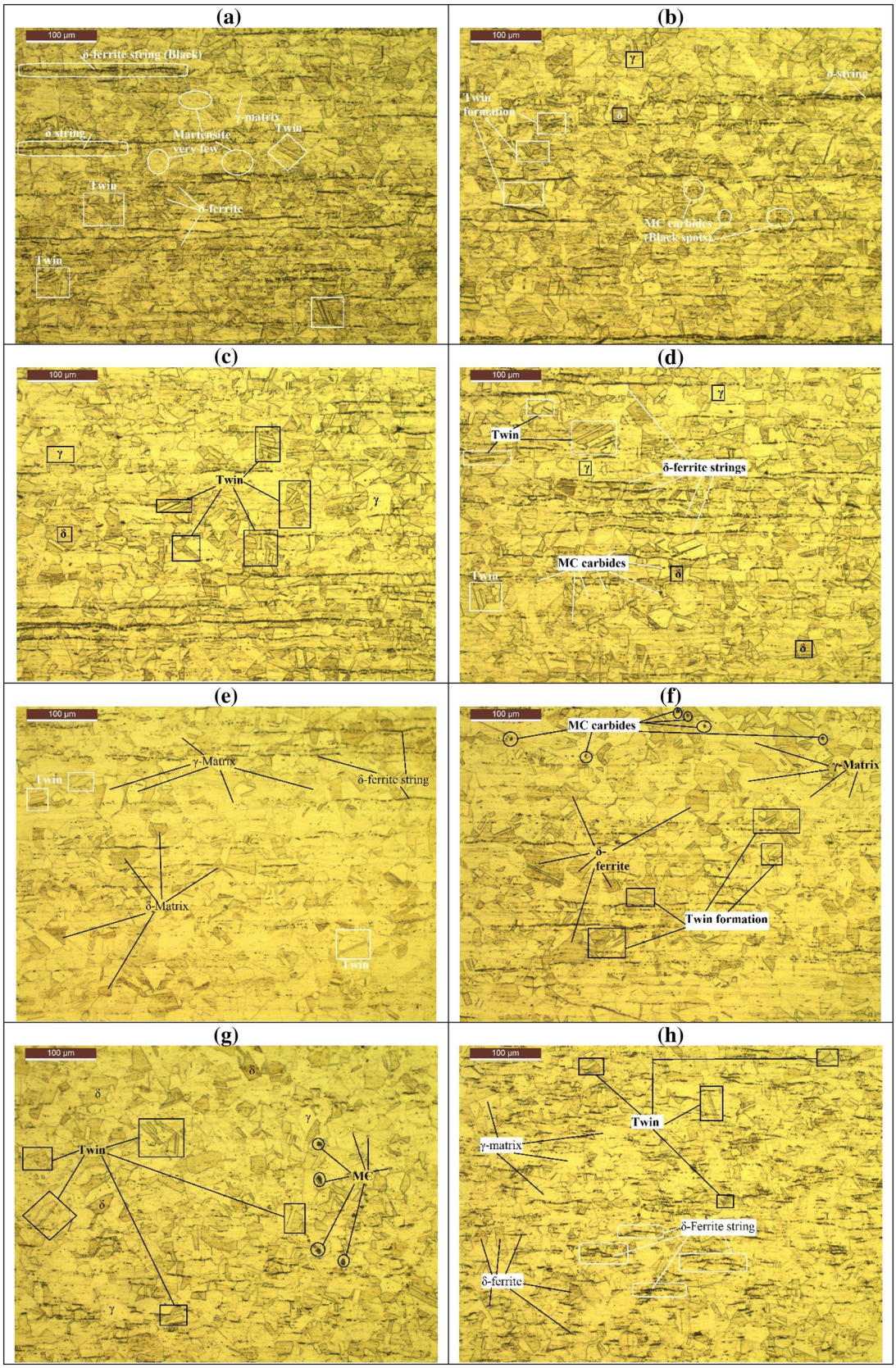

Fig. 2 Microstructure of eight samples: **a** Original sample; **b** Water quenched; **c** Oil quenched; **d** Air cooled; **e** Sand cooled; **f** Brine quenched; **g** Air + water cooled; **h** Air + oil cooled

has been selected which is a highly favorable condition for carbide formation.

It has been investigated that the morphology of M23C6 depends on temperature and soaking time. At low degree of temperatures (> 600 °C), the appearance of carbide is thin and sheet-like. It gets a dendritic shape at grain boundaries when the temperature range becomes 600 to 700° C. By increasing the soaking time, the carbide precipitates become thick and coarse. At temperatures higher than 700 °C, M23C6 takes the shape of discrete globules which is further affected by the boundary orientation of γ-γ and γ-δ [22]. M23C6 formed at a low-temperature range is highly harmful in view of IGC occurrence.

In this study, the M23C6 was observed in the grain boundaries as well as in γ-matrix. These carbides are nearly spherical in shape. The black-colored spots in the images can be resembled as metal-carbides (Fig. 3).

The microstructural images were captured at 1000X to observe carbide formation at grain boundaries. All the images are shown in Fig. 3(a-h). In the original sample, the intergranular M23C6 carbides were observed in the form of black globules. Also, a small portion between γ-δ grain boundaries was containing a number of black spots. It resembles as σ-phase which further is a mixture of newly formed δ (black) and γ (bright). The water-quenched sample (Fig. 2b) also showed numerous carbides and σ formed at the γ-δ interface. In addition, a very small appearance of martensite was observed at the γ-grain. The oil-quenched sample (Fig. 2c) is showing a clear view of M23C6 precipitation at the grain boundary. Also, the twin formation is clearly visible in this sample. Both the air-cooled, and sand-cooled samples showed M23C6 carbides and δ-ferrite strings (Fig. 2d, e). All the above microstructural appearances are the same in the brine-water quenched sample. Also, σ formation was noted in the sample (Fig. 2f). In addition, the next two samples, Air + water and Air + oil cooled samples, possess a similar distribution of σ at grain boundaries (Fig. 2g and h).

(ii) By SEM: The FESEM machine, JEOL make Japan, was used for studying the microstructural changes in the steel. Under this, a backscattered electron detector was utilized for identifying the phases by their color contrast. Due to the varying atomic number of different phases, they can easily be recognized by their brightness/darkness differences. The presence of γ and δ can be recognized as the bright and dark appearance of grains in SEM images. The black colored δ-ferrite strings are the same as observed by LOM. The intergranular $M_{23}C_6$ formation is clearly visible in SEM images. According to Bai et al. (2015) [23], these carbides are responsible for intergranular corrosion (IGC). Along with these, some amount of porosity in γ grains has been reported in water and brine-quenched samples. These porous surfaces are due to pitting corrosion. σ-phase was reported in Air + water and Air + oil cooled samples.

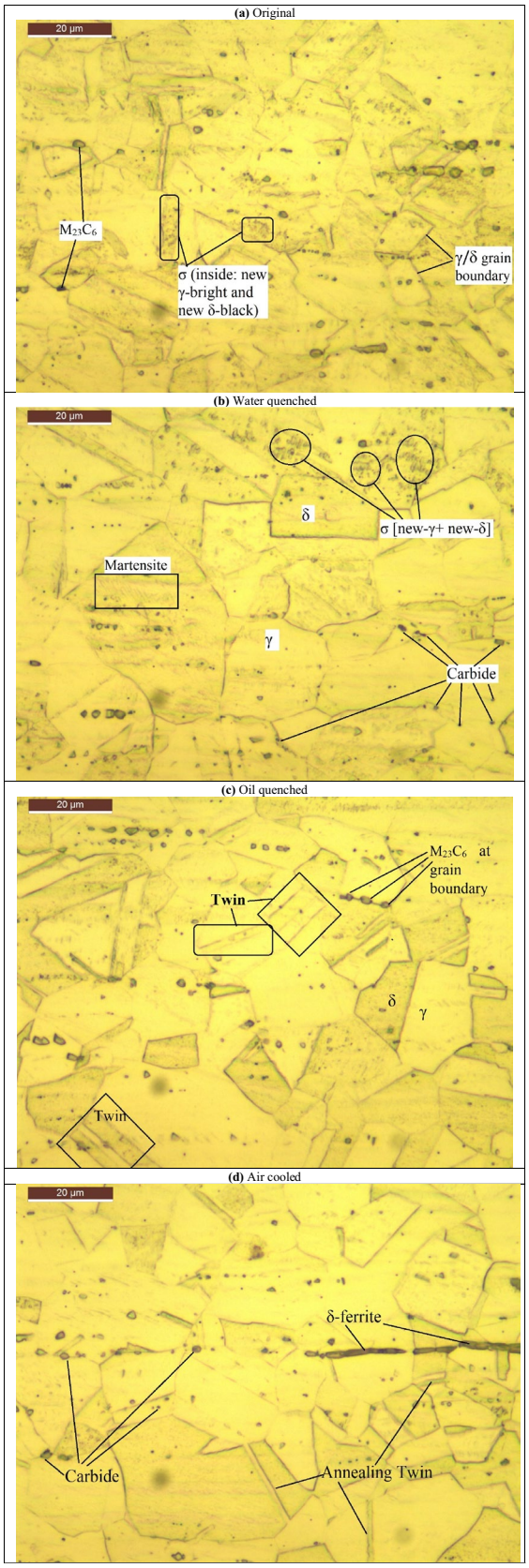

Fig. 3 Microstructure at 1000X: **a** Original sample; **b** Water quenched; **c** Oil quenched; **d** Air cooled; **e** Sand cooled; **f** Brine quenched; **g** Air + water cooled; **h** Air + oil cooled

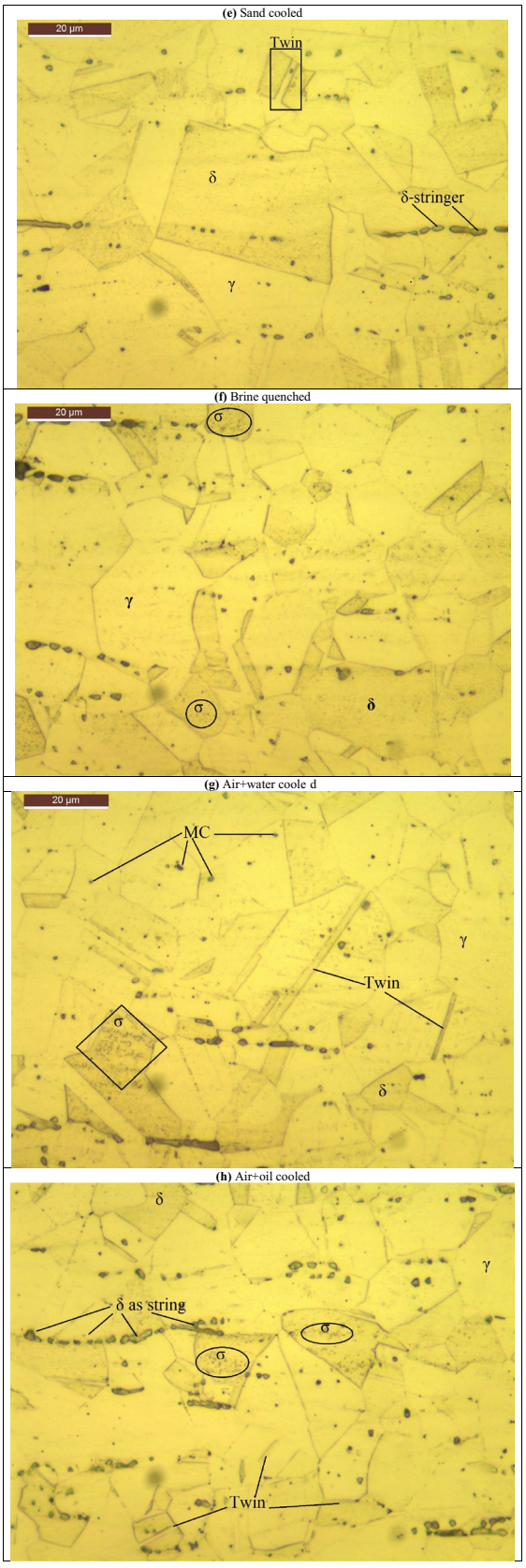

Fig. 3 (continued)

This phase was mainly reported in the δ-grain adjacent to γ-boundary. The recognition of the σ-phase is as per the results obtained by [23] (Fig. 4).

XRD Analysis

XRD analysis was carried out to check the intensities of austenite and ferrite phases present in all the samples. Figure 5 is showing the XRD peaks of all samples. All the samples have shown similar patterns of spikes of austenite (FCC) and ferrite (BCC). The formation of oxides, like Cr_2O_3 and Fe_2O_3, was not observed in XRD peaks. This means the pitting that occurred in austenite grains (of brine-quenched and water-quenched samples) is negligible. However, the XRD peaks are providing a large difference in the level of intensity (CPS) of both γ and δ phases in various samples.

EDS mapping

Elemental analysis was done on each sample to observe the possible changes of constituent elements after heat treatment. Elemental mapping along with EDS was carried out through the same FESEM instrument as discussed above. Eight different elements were mainly notified in the study. They are- C, O, Si, Cr, Mn, Fe, Co, and Ni. The elemental mapping is showing similar results for all eight samples, i.e., 55% Fe, 23% Cr, and 5% Ni. However, the EDS spectra is showing a minor change in Wt% of Cr in heat treated sample. In the original sample, Cr is present in the amount of 18.3% by weight. The brine quenched sample has shown the 18% (Wt%) of Cr. The presence of these elements in all the samples is shown in Fig. 6.

Hardness analysis

The influence of heat treatment on the hardness of samples was analyzed by conducting a micro-Vickers hardness test under 300 gm loading. A total of four indentations were made on each sample and then an average value of hardness was measured in each condition. Table 1 is showing the hardness values in every sample. A comparative bar chart is shown in Fig. 7. For an untreated sample, the hardness value is 168.5 HV. Sand cooling, air cooling, and brine quenching methods had reduced the hardness of the samples by 3.4%, 8.6%, and 5% respectively whereas water quenching, oil quenching, Air + water and Air + oil cooling methods had increased the hardness of the samples by 7.4%, 0.6%, 5.6%, and 2.2% respectively. The highest hardness was reported in the water-quenched sample. This result is opposite to the discussion derived in [2].

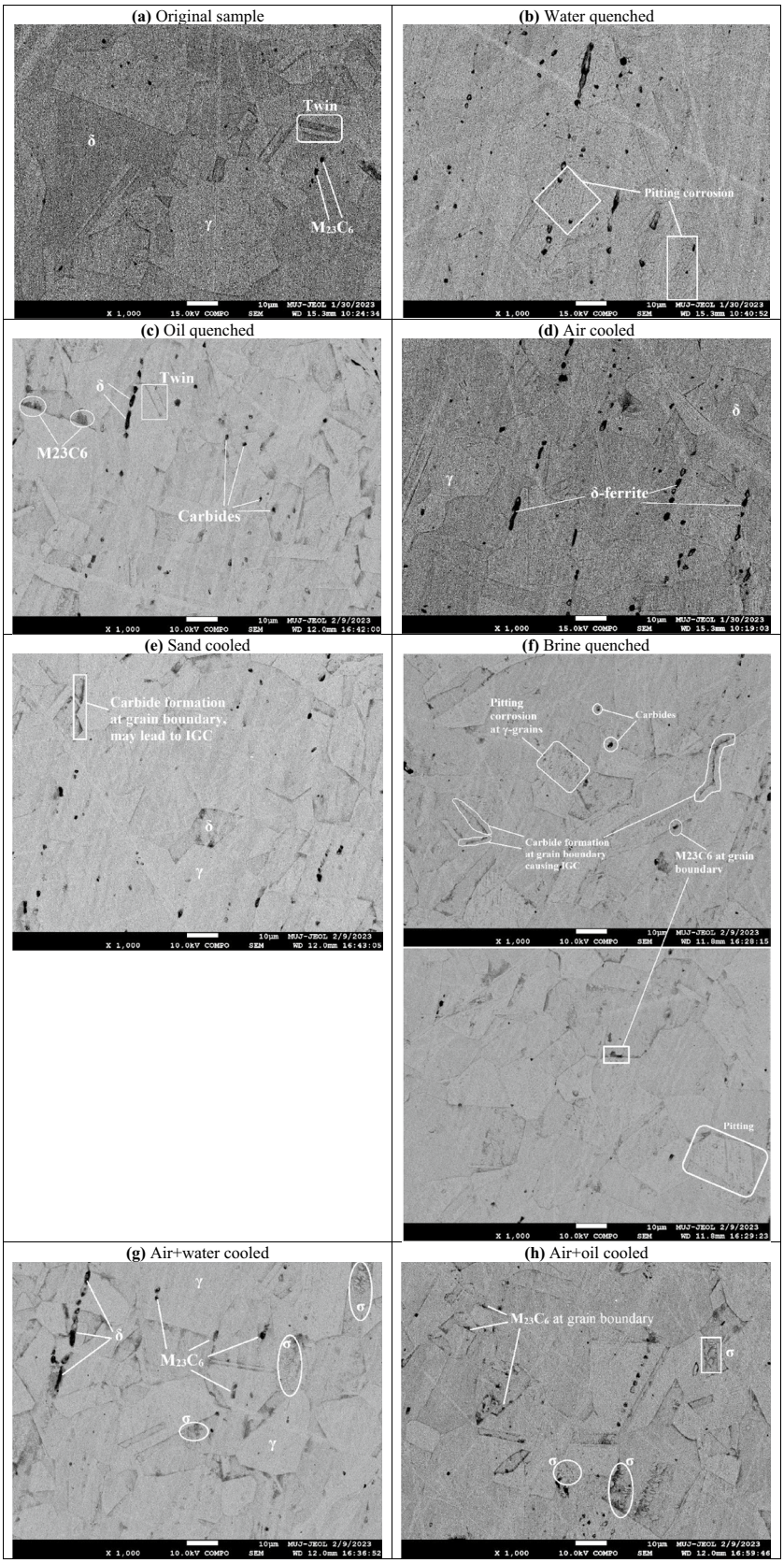

Fig. 4 SEM-BSE images of all the samples

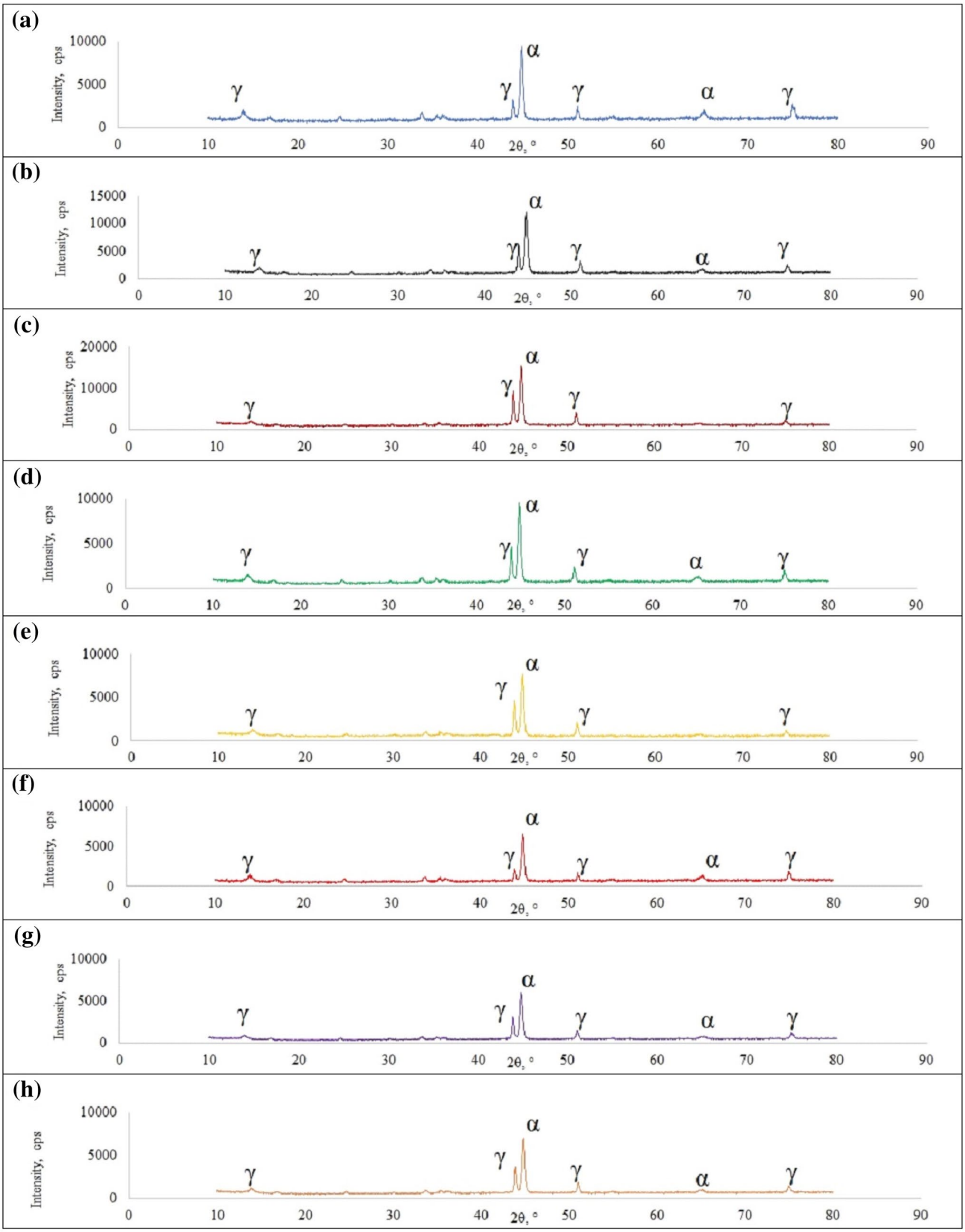

Fig. 5 XRD analysis: **a** Original sample; **b** Water quenched; **c** Oil quenched; **d** Air cooled; **e** Sand cooled; **f** Brine quenched; **g** Air + water cooled; **h** Air + oil cooled

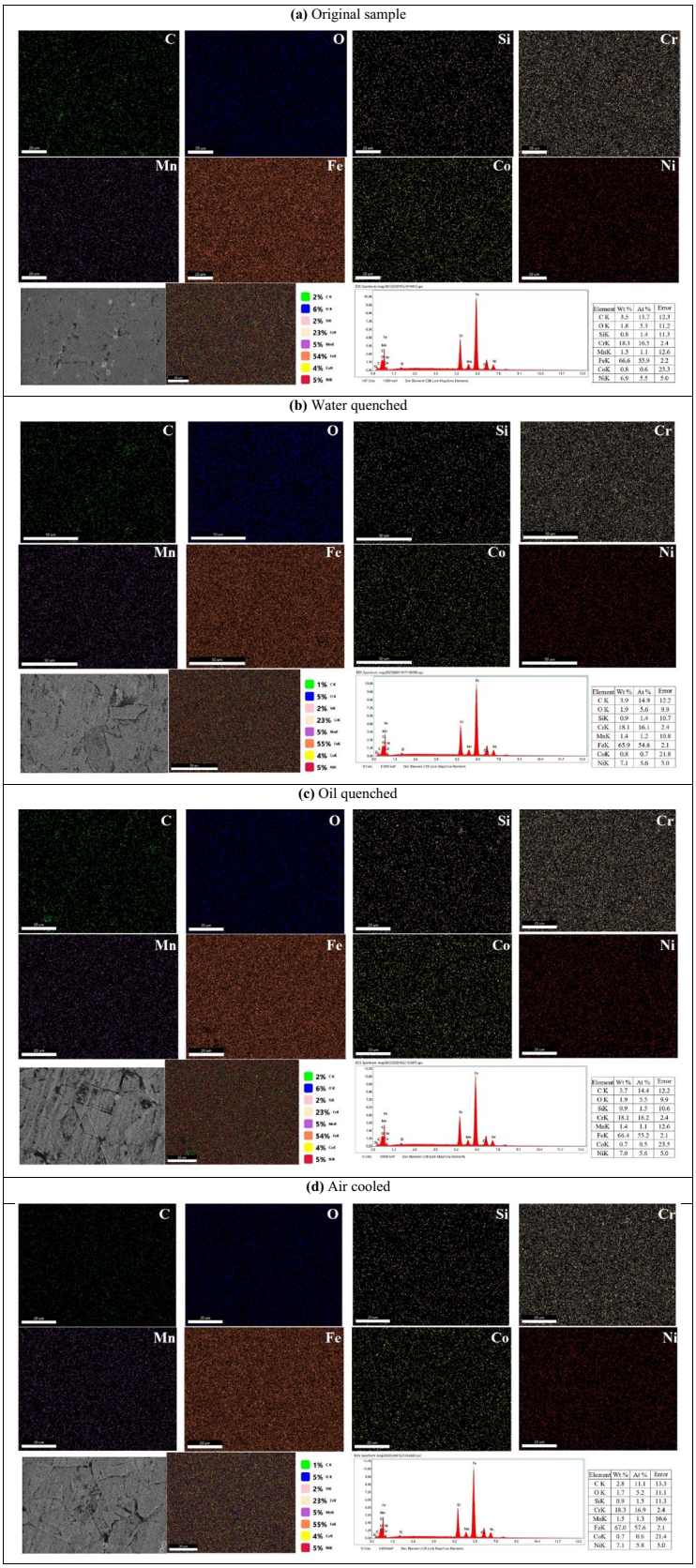

Fig. 6 Elemental mapping and EDS of eight SS samples

Fig. 6 (continued)

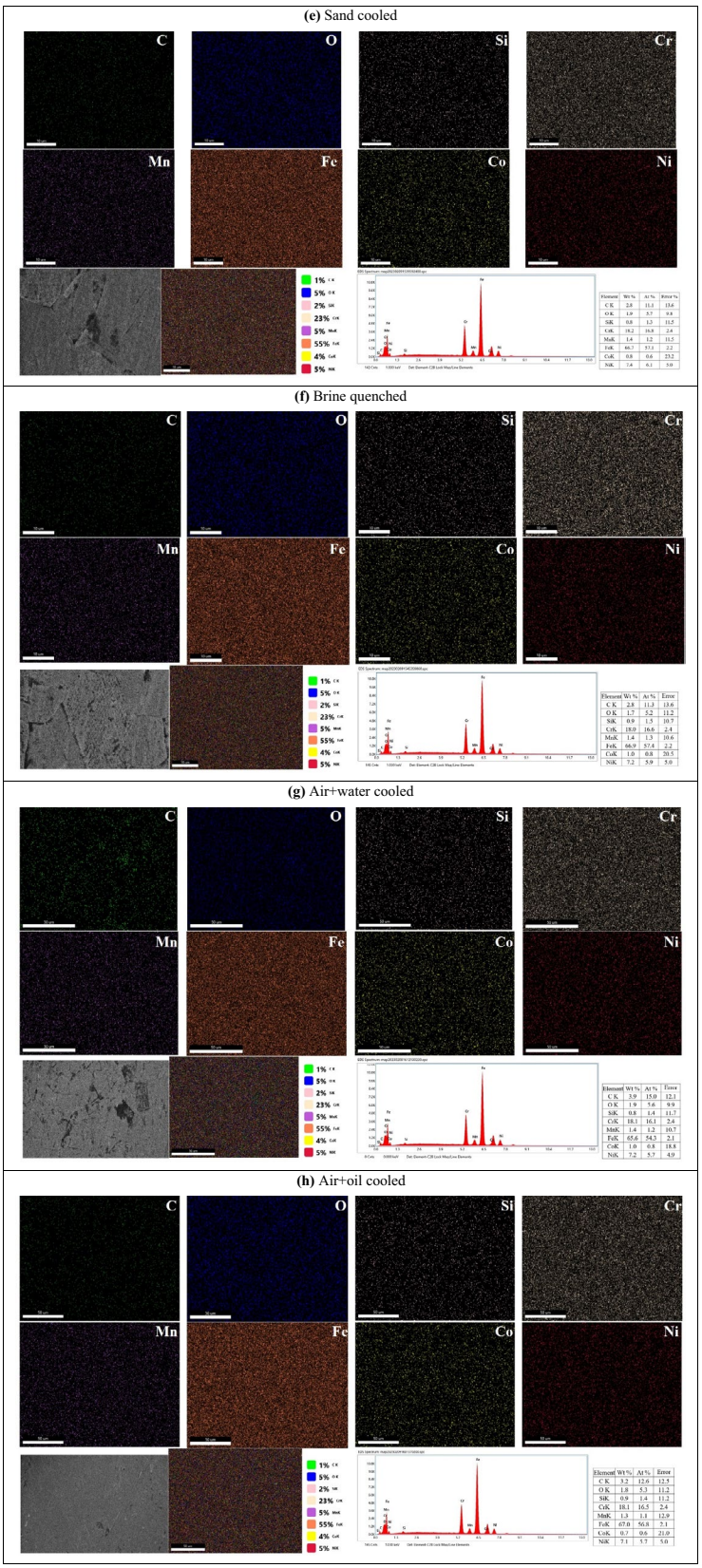

Table 1 Hardness test on samples

Sr. No	Sample	Hardness Values in HV300gms	Average Hardness (HV)
1	Original	163, 171, 174, 166	168.5
2	Water quenched	183, 187, 179, 175	181
3	Oil quenched	165, 173, 172, 168	169.5
4	Air-cooled	160, 149, 151, 156	154
5	Sand cooled	167, 164, 161, 159	162.75
6	Brine quenched	165, 155, 157, 163	160
7	Air + Water cooled	178, 183, 179, 175	178
8	Air + Oil cooled	169, 176, 171, 173	172.25

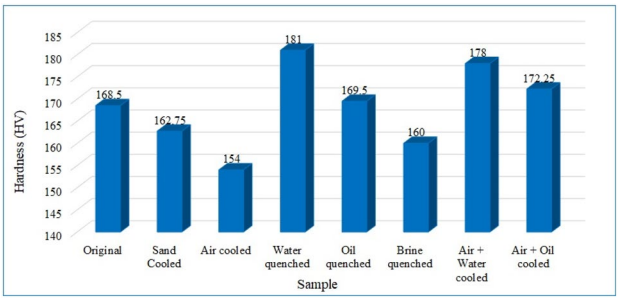

Fig. 7 Comparative analysis of hardness

Conclusion

In this work, an attempt has been made to investigate the effects of various heat treatments on the microstructural attributes and hardness of austenitic stainless steel (SS-304). According to the elemental mapping results, the steel samples under study possess 23% Cr and 5% Ni, which makes them highly corrosion-resistant. A total of eight SS samples were taken. Out of these, seven were undergone through heat treatment and then they were subsequently cooled in different cooling media. The following conclusions are made based on this work:

- The LOM images reveal that all the samples possess similar attributes of γ and δ- phases. The appearance of the δ-stringer is irrespective of any heat treatment methods. The sign of an annealing twin is common in all the samples. A small indication of martensite formation in the γ-phase has been reported in Original and Water-quenched samples.
- The appearance of σ-phase in δ ferrite and $M_{23}C_6$ formation at γ-δ grain boundary has been established by FESEM-BSD images. σ-phase has been mainly reported in both the stepped cooled samples, i.e., Air + water and Air + oil cooled samples.
- BSD images of brine quenched sample clearly reveal the phenomena of pitting on γ-matrix. Pitting has been recognized as a porous surface of individual γ-grain. A very small reduction of Wt% of Cr has been noted in the EDS spectra of the brine sample, although no peak of oxide formation is achieved during XRD analysis.
- As per XRD results, there is no additional compound formed in the steel sample during heat treatment.
- Some variation in hardness values have been recorded in samples. In comparison with the original sample, the water-quenched sample has shown an increment of 7.4% in hardness whereas a reduction of 8.6% has been reported in the air-cooled sample.
- The present study only focuses on different cooling rates while the treatment time and temperature are common to all the samples. In future work, a significant variation in aging time and temperature can be considered for better output.

Author contributions Both authors contributed to the study, conception, and design. All the experimental works were performed by SM. The result analysis and manuscript preparation were done by SD. Both authors have read and approved the manuscript before the submission.

Funding The authors declare that no funds, grants, or other support were received during the preparation of this manuscript.

Declarations

Competing interests The authors have no relevant financial or non-financial interests to disclose.

References

1. P. Wang, Y. Zhang, D. Yu, Microstructure and mechanical properties of pressure-quenched SS304 stainless steel. Materials **12**, 290 (2019). https://doi.org/10.3390/ma12020290
2. Metallographic preparation of stainless steel. https://www.struers.com/en/Knowledge/Materials/Stainless-Steel. Accessed 07 Mar 2023
3. A.T. Zeuner, L. Ewenz, J. Kalich, S. Schöne, U. Füssel, M. Zimmermann, The influence of heat treatment on the microstructure, surface roughness and shear tensile strength of AISI 304 clinch joints. Metals **12**, 1514 (2022). https://doi.org/10.3390/met12091514
4. S. Sirohi, S.M. Pandey, A. Swierczynska, G. Rogalski, N. Kumar, M. Landowski, D. Fydrych, C. Pandey, Microstructure and mechanical properties of combined GTAW and SMAW dissimilar welded joints between inconel 718 and 304L austenitic stainless steel. Metals **13**, 14 (2023). https://doi.org/10.3390/met13010014
5. P.V. Reddy, B.V. Reddy, P.J. Ramulu, Effect of heat treatment temperatures on formability of SS 304 during tube hydroforming

process. SN Appl. Sci. **2**, 205 (2020). https://doi.org/10.1007/s42452-020-2026-7
6. H. Essoussi, S. Elmouhri, S. Ettaqi, E. Essadiqi, Heat treatment effect on mechanical properties of AISI 304 austenitic stainless steel. Procedia Manuf. **32**, 883–888 (2019). https://doi.org/10.1016/j.promfg.2019.02.298
7. S. Dewangan, S. Chattopadhyaya, Analysing effect of quenching and tempering into mechanical properties and microstructure of 304-SS welded plates. Acta Metallurg. Slovaca **28**(3), 140–146 (2022)
8. J.W. Fu, Y.S. Yang, J.J. Guo, J.C. Ma, W.H. Tong, Microstructure evolution in AISI 304 stainless steel during near rapid directional solidification. Mater. Sci. Technol. **25**(8), 1013–1016 (2009). https://doi.org/10.1179/174328408X317093
9. S.A. Rizvi, Effect of heat input on microstructural and mechanical properties of AISI 304 welded joint via MIG welding. IJE Trans. C Aspects **33**(9), 1811–1816 (2020)
10. R.I.M. Essam, Microstructure, wear and corrosion characteristics of 304 stainless steel laser cladded with titanium carbide. Int. J. Eng. Res. Technol. **4**(8), 552 (2015)
11. Z. Brytan, J. Niagaj, Effect of isothermal heat treatment at 650, 750 and 850 on the microstructures of lean duplex stainless steel S32101 welds. Chiang Mai J. Sci. **40**(5), 874–885 (2013)
12. L. Kosec, M. Gojić, S. Kožuh, B. Kosec, G. Dražić, Š. Šavli. The effect of long-term annealing at elevated temperature on microstructure and hardness of heat-resistant steel. Materials Science Forum, 782, Trans Tech Publications, Ltd., 2014, pp. 209–214. doi:https://doi.org/10.4028/www.scientific.net/msf.782.209.
13. J. Zmywaczyk, A. Debski, M. Zieliński, M. Preiskorn, P. Koniorczyk, J. Sienkiewicz, Effect of microstructure on thermophysical properties of heat-treated duplex steel. Materials. **14**(20), 6043 (2021)
14. J. Fu, C. Xia, Microstructure evolution and mechanical properties of X6CrNiMoVNb11-2 stainless steel after heat treatment. Materials **14**(18), 5243 (2021). https://doi.org/10.3390/ma14185243
15. Y. Wang, S.L. Tay, S. Wei, C. Xiong, W. Gao, R.A. Shakoor, R. Kahraman, Microstructure and properties of sol-enhanced Ni-Co-TiO_2 nano-composite coatings on mild steel. J. Alloys Comp. **649**, 222–228 (2015). https://doi.org/10.1016/j.jallcom.2015.07.147
16. S. Geng, J. Sun, L. Guo, H. Wang, Evolution of microstructure and corrosion behavior in 2205 duplex stainless steel GTA-welding joint. J. Manuf. Process. **19**, 32–37 (2015). https://doi.org/10.1016/j.jmapro.2015.03.009
17. K. Prasad, D.K. Dwivedi, Some investigations on microstructure and mechanical properties of submerged arc welded HSLA steel joints. Int. J. Adv. Manuf. Technol. **36**, 475–483 (2008). https://doi.org/10.1007/s00170-006-0855-1
18. L. Zhang, A. Ma, J. Jiang, X. Jie, Effect of processing methods on microhardness and acid corrosion behavior of low-carbon steel. Mater. Des. **65**, 115–119 (2015). https://doi.org/10.1016/j.matdes.2014.09.010
19. J. Zhan, M. Li, J. Huang, H. Bi, Q. Li, H. Gu, Thermal fatigue characteristics of type 309 austenitic stainless steel for automotive manifolds. Metals **9**, 129 (2019). https://doi.org/10.3390/met9020129
20. V.A. Rao, R. Deivanathan, Experimental investigation for welding aspects of stainless steel 310 for the process of TIG welding. Procedia Eng. **97**, 902–908 (2014). https://doi.org/10.1016/j.proeng.2014.12.365
21. G. F. V. Voort, G. M. Lucas, E. P. Manilova. Metallography and Microstructures of Stainless Steels and Maraging Steels. ASM Handbook, Volume 9: Metallography and Microstructures G.F. Vander Voort, editor, p670–700. DOI: https://doi.org/10.1361/asmhba0003767
22. R. Stickler, A. Vinckier, Morphology of grain-boundary carbides and its influence on intergranular corrosion of 304 stainless steel. Trans. ASM **54**, 362–380 (1961)
23. G. Bai, S. Lu, D. Li, Y. Li, Intergranular corrosion behavior associated with delta-ferrite transformation of Ti-modified Super304H austenitic stainless steel. Corros. Sci. **90**, 347–358 (2015). https://doi.org/10.1016/j.corsci.2014.10.031